
Article:
Robinson, Martin Paul, Fitton, Laura Catherine, Little, Aimee Patrice et al. (2019) Dielectric Replica Measurement: A New Technique for Obtaining the Complex Permittivity of Irregularly Shaped Objects. Measurement Science and Technology. 045902. ISSN: 0957-0233

https://doi.org/10.1088/1361-6501/ab0466

Dielectric Replica Measurement: A New Technique for Obtaining the Complex Permittivity of Irregularly Shaped Objects

Dr Martin Robinson[1], Dr Laura Fitton[2], Dr Aimee Little[2], Dr Sam Cobb[2], Dr Steve Ashby[3]

1. Department of Electronic Engineering
University of York

2. Department of Archaeology / Hull-York Medical School
University of York

3. Department of Archaeology
University of York

Abstract

Dielectric measurements provide valuable information about the properties of materials, and could be used to classify and identify the source of objects, in fields such as archaeology. Current methods of identification are all partly destructive, so an innovative electromagnetic method developed by the authors, based on resonant cavity perturbation (RCP), provides an attractive, non-destructive alternative. A problem with traditional RCP is that the changes in frequency and Q-factor vary with the object's shape; however we overcome this by creating a replica of the object, from a material whose dielectric properties are known. Then, by combining three separate perturbations with orthogonal field directions, due firstly to the object and then to its replica, we eliminate the shape dependency, and thus determine the object's dielectric constant and loss factor. After developing the theory of this novel DRM technique, we demonstrate the principle using a set of geometric shapes made in both polytetrafluoroethylene (PTFE) and a 3D printed material. Further measurements then enable second-order terms to be included in the model, improving its accuracy. Finally, DRM is shown to be capable of distinguishing two irregularly shaped objects of different materials. Potential applications of DRM include determining the provenance of pottery, glasses and flints, and distinguishing ivory from bone. These would be of interest to customs and environmental agencies, as well as museum curators and archaeologists.

Keywords

Dielectric measurement, complex permittivity, archaeology, artefact, non-destructive testing, resonant cavity, network analyser, 3D printing.

1. Introduction

Dielectric measurements give us useful information about the properties of materials (Kaatze 2012). Such measurements can be made at frequencies ranging from DC to microwaves, and have numerous and varied applications in characterising and distinguishing materials, notably for organic matter where they can be used to estimate water content (Kraszewski and Nelson 1990, Nuutinen et al. 2004).

Liquids are relatively easy to measure (Gregory and Clarke 2006), as these can be poured into a measurement cell, which forms part of a transmission line. Alternatively, an open-ended coax sensor, attached to the end of a coaxial cable, can be immersed or brought up to the liquid surface.

Solids are harder to deal with. If a solid object is large enough, one can machine a flat surface on it, and apply a coaxial probe, as with liquids, although it can be hard to avoid an air gap in between.

Alternatively the material can be formed into a simple geometric shape such as a pill-shaped cylinder, and placed it in a resonant cavity. The dielectric properties at a single frequency can then be obtained by resonant cavity perturbation (RCP), a well-established technique (Horner et al 1946) that is explained in the following section.

But traditional RCP is not feasible if the objects under test are irregular and cannot be destructively modified, for example excavated artefacts that need identifying. The reason is that changes in the frequency of the resonance, and its Q-factor (sharpness), are determined not only by the dielectric properties of the object, but also by its shape. If we could eliminate the effect of shape, we could determine the object's dielectric constant and loss factor. These values would then be compared with a database of known dielectric properties in order to identify the material.

Various researchers have found that the shape factor can be reduced by combining measurements with the test object in two or more orientations, e.g. Kraszewski and Nelson (1990) looking at seeds, and Oldroyd et al (2015) measuring total body water (TBW) in human subjects. In this paper we demonstrate a novel method of removing the shape factor completely, by comparing to an object of the same shape and known dielectric properties, as illustrated in Figure 1. We develop the theory of this new method and validate it by comparing sets of geometric solids fabricated from two different dielectric materials. From further measurements we derive second-order corrections to the model, enhancing its accuracy. Finally we test the system with irregularly shaped objects of materials likely to be found in archaeological excavations.

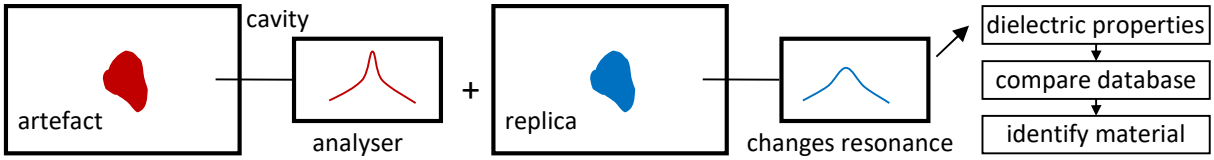

Figure 1. Principle of Dielectric Replica Measurement (DRM)

This new method, invented by the authors, holds considerable potential for the heritage sector where non-destructive and low-cost methods of identifying archaeological materials are few. Destructive methods such as chemical analysis and laser ablation inductively coupled mass spectrometry (LA-ICP-MS) have been employed to identify the source of black chert stones (Evans et al. 2010) and the provenance of ceramics (Stoner 2016), while ancient DNA (aDNA) analysis and zooarchaeology by mass spectrometry (ZooMS) have helped identify the origin of antler and bone artefacts (von Holstein 2014). Other materials, for which small variations in chemical composition can aid their identification, are glass (Freestone 2006) and steatite (soapstone) (Truncher et al. 1998). Müller and Reiche (2011) have used such variations to differentiate ivory and bone. For all these materials, the changes in composition will affect their dielectric properties, making DRM a potential alternative.

2. Theory

Complex permittivity is defined as $\varepsilon^*=\varepsilon'-j\varepsilon''$ where ε' and ε'' are respectively the dielectric constant and loss factor; the ratio of these is called the loss tangent. At frequency f, the loss factor is related to AC conductivity σ by $\sigma=2\pi f\varepsilon''\varepsilon_0$ where ε_0 is the permittivity of free space.

Harrington's theory of resonant cavity perturbation (Harrington 1961) shows that the dielectric properties of a small sample of material placed within a resonant cavity are related the changes in resonant frequency and Q-factor, provided that the field pattern within the cavity is not excessively perturbed by the sample and that the sample is totally within the cavity. Kraszewski and Nelson (1996) define a complex frequency shift $\Delta\Omega$ in terms of the change Δf of the resonant frequency f_0

and the change in the reciprocal of its Q-factor. When a small sample is placed at the centre of a resonant cavity, they predict that:

$$\Delta\Omega = \frac{\Delta f}{f_0} + \frac{1}{2} j\Delta\left(\frac{1}{Q}\right) = -\frac{1}{2}\frac{1}{C}\frac{v_s}{v_c}\frac{\varepsilon^* - 1}{\left[1 + A(\varepsilon^* - 1)\right]} \qquad (1)$$

where v_s/v_c the ratio of sample volume to cavity volume, C is a geometrical constant and A is the depolarisation factor. Ideally v_s/v_c should be less than 0.001, however practical experience shows that reasonably accurate measurements are possible for larger sample volumes, especially if higher-order terms are included (Robinson et al 2010, Robinson and Clegg 2008).

The depolarisation factor depends on the shape and orientation of the sample and has a value between zero and one. Values along three orthogonal axes A_x, A_y, A_z relative to the E-field are given for some simple geometries in Table 1: it can be seen that as a sample becomes more elongated A_x tends to zero, while as it becomes flattened A_x approaches one. Note also that

$$A_x + A_y + A_z = 1 \qquad (2)$$

Table 1. Depolarisation factors for E-field vector oriented along *x*, *y* and *z*-axes

shape	A_x	A_y	A_z
long cylinder parallel to *x*-axis	0	½	½
sphere	⅓	⅓	⅓
thin slab normal to *x*-axis	1	0	0

From (1) the complex permittivity is given by:

$$\varepsilon^* = 1 - \frac{\Delta\Omega}{A\Delta\Omega + \left(v_s / 2Cv_c\right)} \qquad (3)$$

If the depolarisation factor A is zero then the real and imaginary parts separate, so ε' becomes a function of Δf, and ε'' a function of $\Delta(1/Q)$. For all other shapes, we a get complex mapping of $\Delta\Omega$ to ε^*, with the perturbation depending on the shape as well as on the dielectric properties.

To eliminate the dependence on shape we note that

$$A = \frac{1}{\varepsilon^* - 1} - \frac{v_s}{2Cv_c}\frac{1}{\Delta\Omega} \qquad (4)$$

If we make three separate measurements, with the E-field aligned first along the *x*-axis, then the *y*-axis and finally the *z*-axis, we will obtain three complex perturbations $\Delta\Omega_x$, $\Delta\Omega_y$, and $\Delta\Omega_z$. Summing the corresponding values of A gives

$$A_x + A_y + A_z = 1 = \frac{3}{\varepsilon^* - 1} - \frac{v_s}{2Cv_c}\left(\frac{1}{\Delta\Omega_x} + \frac{1}{\Delta\Omega_y} + \frac{1}{\Delta\Omega_z}\right) \qquad (5)$$

and hence

$$\varepsilon^* = 1 - 3\left[1 + \frac{v_s}{2Cv_c}\left(\frac{1}{\Delta\Omega_x} + \frac{1}{\Delta\Omega_y} + \frac{1}{\Delta\Omega_z}\right)\right]^{-1} \tag{6}$$

which is now independent of sample shape, but not of sample volume.

The measurement of these $\Delta\Omega_{x,y,z}$ can be achieved either (a) by rotating the sample within the cavity, or (b) by taking advantage of symmetry when designing the cavity, and relying on further, degenerate modes at the same (or very close) frequencies, but with their E-field vectors aligned at right angles to the first mode. This is a valid approach because the cavity volume remains constant as well as the measurement frequency. In our experiments we use a combination of both methods, rotating the sample to get the second perturbation, and switching modes to get the third.

To remove the other unknown constants in (6), we can define a complex factor

$$\alpha = \frac{\varepsilon^* - 1}{\varepsilon^* + 2} = \frac{2Cv_c}{v_s}\left(\frac{1}{\Delta\Omega_x} + \frac{1}{\Delta\Omega_y} + \frac{1}{\Delta\Omega_z}\right)^{-1} \tag{7}$$

Congruent shapes will have the same C and v_s, and v_c is also constant. Hence we can take two samples of the same shape and volume, measure them both in the cavity to obtain all three perturbations, and then find the complex permittivity of the second material from that of the first:

$$\alpha_2 = \alpha_1 \frac{\frac{1}{\Delta\Omega_{x,1}} + \frac{1}{\Delta\Omega_{y,1}} + \frac{1}{\Delta\Omega_{z,1}}}{\frac{1}{\Delta\Omega_{x,2}} + \frac{1}{\Delta\Omega_{y,2}} + \frac{1}{\Delta\Omega_{z,2}}} = \alpha_1 \frac{\sum \Delta\Omega_1^{-1}}{\sum \Delta\Omega_2^{-1}} \tag{8}$$

where subscript 1 refers to the known material and 2 to the unknown; the combined shift in complex frequency $\sum \Delta\Omega^{-1}$ is summed over the x, y and z orientations, and $\alpha_1 = (\varepsilon_1^* - 1)/(\varepsilon_1^* + 2)$.

Finally the required complex permittivity of the unknown material is

$$\varepsilon_2^* = \frac{1 + 2\alpha_2}{1 - \alpha_2} \tag{9}$$

Furthermore, in the case where the objects are the same shape but different sizes, we can correct (6) for the volumes of the samples:

$$\alpha_2 = \alpha_1 \frac{v_{s,1}}{v_{s,2}} \frac{\sum \Delta\Omega_1^{-1}}{\sum \Delta\Omega_2^{-1}} \tag{10}$$

where again the subscripts 1, 2 refer to known and unknown samples.

For some simple shapes, a replica could be made by conventional manufacturing methods. However for complex, irregular geometries, it will be more convenient to scan the surface of the object and to produce a copy by means of additive manufacturing, commonly known as 3D printing.

3. Materials for initial tests

For the initial measurements to test the DRM concept, we used a 3D-printed material as the unknown, and a polymer whose dielectric properties are well known as the calibration material.

Sets of simple geometric shapes were made from (a) polytetrafluoroethylene (PTFE, Teflon), by conventional techniques of boring and milling, and (b) an acrylic polymer produced by 3D printing using a Objet 24 machine (Stratasys) (see Figure 2).

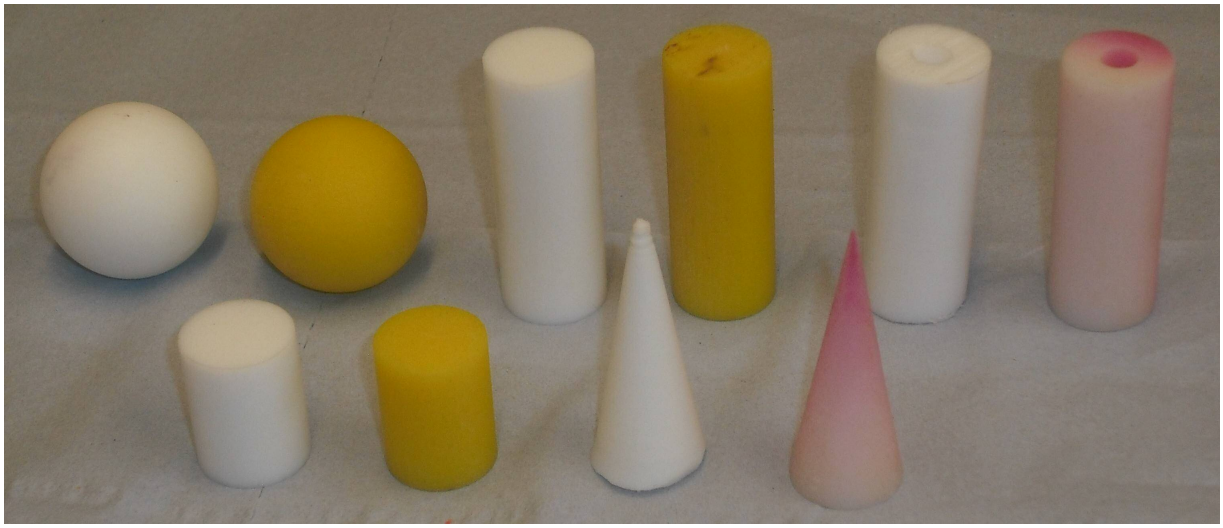

Figure 2. Objects used to test Dielectric Replica Measurement (DRM), with PTFE versions to left of 3D-printed acrylic copies. The sphere at the top left is 25.6mm in diameter.

Table 2 shows the dimensions, mass and volume of the PTFE and acrylic shapes. Although the intention was to create exact replicas, there were slight differences in the dimensions, which were measured with Vernier callipers. Of the objects in the table, A-E were made for this study, while F-H were used opportunistically for extra measurements but were only available in one material

Table 2. dimensions of plastic geometric shapes

Solid	PTFE, $\varepsilon^* = 2.1 - 0j$		3D-printed acrylic, ε^* unknown	
	shape	volume (cm^3)	shape	volume (cm^3)
A	sphere dia. 25.6mm	8.78	sphere dia. 25.4mm	8.58
B	short cylinder dia. 15.2mm height 20.0mm	3.63	short cylinder dia. 14.9mm height 20.1mm	3.50
C	medium cylinder dia. 15.2mm height 40.1mm	7.28	medium cylinder dia. 15.0mm height 40.1mm	7.09
D	hollow cylinder dia. 15.2mm inner dia. 4.7mm height 40.2mm	6.60	hollow cylinder dia. 15.0mm inner dia. 5.0mm height 40.0mm	6.38
E	cone dia. 15.3mm height 37.8mm	2.32	cone dia. 14.9mm height 39.5mm	2.30
F	large sphere dia. 31.9mm	17.00	-	-
G	-	-	long cylinder dia. 14.9mm height 80.0mm	14.52
H	long cylinder dia. 15.2mm height 70.0mm	12.70	-	-

4. Cavity perturbation measurements on geometrical shapes

Figure 3 shows the cavity that formed part of our dielectric measurement system. The cavity is an aluminium cylinder, diameter and height both 560mm. It was adapted from a resonant chamber that formed part of a dielectric heating system for re-warming of cryopreserved biological samples (Evans et al., 1992, Rachman et al. 1992, Robinson and Pegg 1999).

As the cavity has a square aspect ratio, its TM010 and TE111 modes should be degenerate, with resonant frequency approximately 430MHz. Both modes have a maximum E-field at the centre of the cavity, as required. However the E-field of the TM010 mode is vertical (*z*-directed) at the cavity centre whereas that of the TE111 mode is horizontal. In the actual design a slight asymmetry separates the frequencies of these modes by a few MHz to prevent cross-coupling.

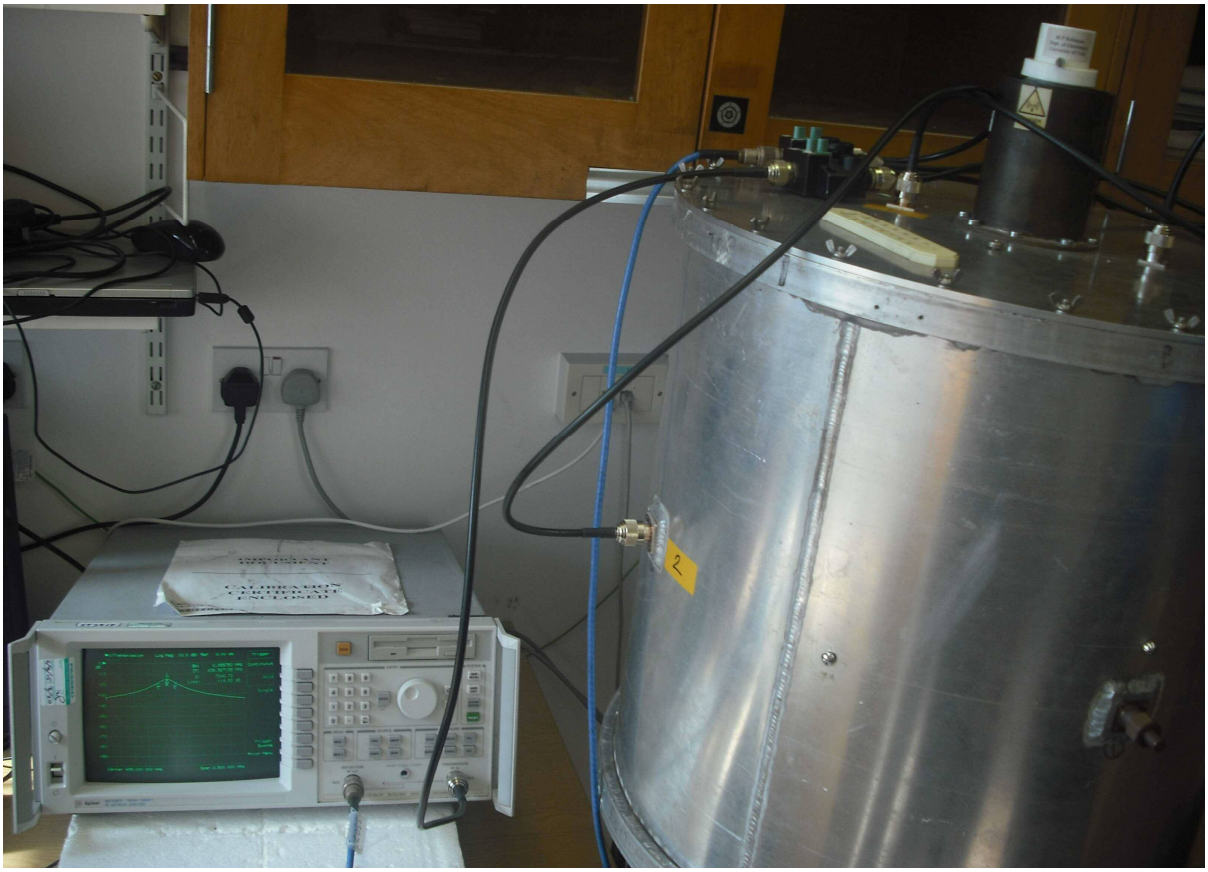

Figure 3. Photograph of cavity (right) connected to VNA (left). One of the connectors probing the horizontal, TE111 mode, for *x*- and *y*-perturbations, can be seen on the left side of the cavity. The end of the rotatable sample holder (white) is at top right.

The cavity is sealed with welded joints and a lid that is attached by multiple screws and wingnuts. A piece of piping, 115m long and 82mm internal diameter, is attached to an aperture in the lid, and acts as a waveguide below its cut-off frequency. This prevents coupling through the aperture while allowing access for samples to be inserted.

The sample holder, as seen in figures 3 and 4, is a length of polypropylene tube, with a cage formed at the end to hold the sample at the cavity centre. The holder can be rotated through 90° to switch between *x* and *y* polarisations, as explained below.

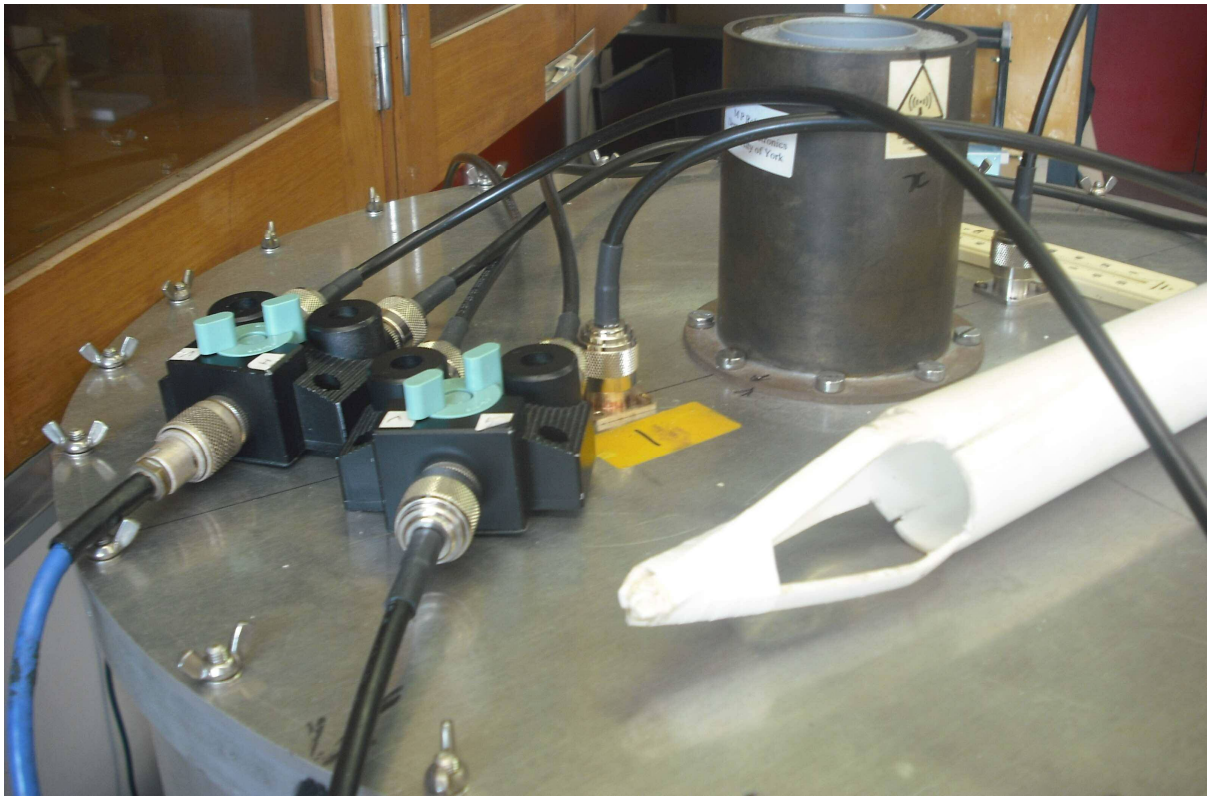

Figure 4. Photograph showing sample holder (white structure on right), RF switches (centre left), below-cut-off waveguide pipe on lid of cavity (top right) and connectors for probing the vertical, TM010 mode, on opposite sides of this pipe.

Pairs of wire antennas, 34mm long, have been attached to N-type connectors in the lid and the sides to couple to two separate cavity modes. The TM010 mode with vertical E-field is excited and detected by antennas in the lid, half between the centre and the edge. This mode has a resonant frequency of 434MHz and a Q-factor of 2900 when the sample holder is empty. Its maximum transmission coefficient S_{21} is -17dB. For the TE111 mode with horizontal E-field, the antennas are on opposite sides of the cylinder, and its frequency, Q and maximum S_{21} are respectively 439MHz, 7500 and -15dB.

Mechanical coaxial switches enable the appropriate pair of antennas to be selected. An 8712ET vector network analyser (VNA) (Agilent) measures the transmission coefficient between each antenna pair, over a narrow band of frequencies (typically 0.5MHz), including the resonant frequency. The number of points is 1601 and the system bandwidth is 250Hz. The VNA automatically determines f_0 from the maximum in S_{21}, and Q from the 3-dB bandwidth of the resonant peak.

Switching to the vertical, TM010 mode gives us the polarisation in the z-direction while the horizontal, TE111 mode initially gives us the x-polarisation. To get the third (y) direction, we utilise the ability of the sample holder to rotate about the axis of the cylindrical cavity: turning it through 90° gives us the y-polarisation. It would technically be possible to add a third pair of antennas to the cavity instead, enabling all three perturbations to be measured on a fixed sample.

The measurement procedure is to first measure f_0 and Q_0 for each of the *x*, *y* and *z* perturbations, with the sample holder empty. Next insert the original sample in the holder, and measure the 'loaded' f_{s1} and Q_{s1} for each direction, by switching and rotating as appropriate. Then remove the sample, re-measure f_0, Q_0, and average these values with the 'empty' measurements made earlier.

The same procedure is then repeated for the replica, taking care to ensure that it lies in the same position in the holder as the original, to give f_{s2} and Q_{s2} for each orientation. Finally, the complex frequency shifts are evaluated and combined, and the complex permittivity of the original is found from the complex permittivity of the replica, using (8) and (9) if the shapes are identical, or (10) and (9) if there are slight differences in volume.

A simpler procedure was used for the geometric shapes in Table 2: these were all axially symmetric and aligned vertically, so we assumed that $\Delta\Omega_x = \Delta\Omega_y$ and only measured two perturbations for each sample. For asymmetric samples (see Section 7 below) we needed all three perturbations, so for these we used the full procedure.

5. Results for simple geometric shapes

Table 3 shows the changes in frequency and Q for the samples in Table 2. Inserting the PTFE and acrylic objects into the cavity shifted the resonant frequencies negatively by 0.012 to 0.19MHz. The PTFE objects had only a small effect on the Q-factors, but the 3D-printed acrylic objects reduced the Q of the resonances by up to 9%.

Table 3. complex frequency shifts for plastic geometric shapes

Solid	PTFE		3D-printed acrylic	
	$\Delta\Omega_x$, $\Delta\Omega_y$	$\Delta\Omega_z$	$\Delta\Omega_x$, $\Delta\Omega_y$	$\Delta\Omega_z$
A	$-1.09\times10^{-4} - 1.21\times10^{-7}j$	$-1.24\times10^{-4} + 4.13\times10^{-7}j$	$-1.65\times10^{-4} + 3.57\times10^{-6}j$	$-1.89\times10^{-4} + 4.79\times10^{-6}j$
B	$-4.27\times10^{-5} - 7.74\times10^{-8}j$	$-5.96\times10^{-5} + 2.92\times10^{-7}j$	$-6.29\times10^{-5} + 1.61\times10^{-6}j$	$-9.54\times10^{-5} + 2.96\times10^{-6}j$
C	$-8.11\times10^{-5} + 6.70\times10^{-9}j$	$-1.26\times10^{-4} + 1.26\times10^{-7}j$	$-1.22\times10^{-4} + 2.54\times10^{-6}j$	$-2.08\times10^{-4} + 6.97\times10^{-6}j$
D	$-7.45\times10^{-5} - 1.06\times10^{-7}j$	$-1.14\times10^{-4} - 3.41\times10^{-8}j$	$-1.11\times10^{-4} + 2.66\times10^{-6}j$	$-1.92\times10^{-4} + 6.65\times10^{-6}j$
E	$-2.81\times10^{-5} + 1.88\times10^{-8}j$	$-4.81\times10^{-5} - 1.16\times10^{-7}j$	$-4.03\times10^{-5} + 1.02\times10^{-6}j$	$-7.21\times10^{-5} + 2.70\times10^{-6}j$
F	$-2.17\times10^{-4} - 4.83\times10^{-7}j$	$-2.31\times10^{-4} + 1.94\times10^{-7}j$		
G	$-1.44\times10^{-4} - 1.70\times10^{-7}j$	$-2.24\times10^{-4} + 1.57\times10^{-7}j$		
H			$-2.36\times10^{-4} + 4.83\times10^{-6}j$	$-4.44\times10^{-4} + 1.62\times10^{-5}j$

Some researchers have reported an increase in Q when very low-loss materials such as PTFE are inserted into the cavity in an RCP measurement (Chen et al. 1999, Sheen, 2007). This effect was not

apparent in our study, and the changes in Q that we observe for this material seem to be due to experimental variation and not statistically significant. A reason could be that the ratio of sample volume to cavity volume, v_s/v_c, was small compared to that in the experiments of the above cited authors, being only 1.7×10^{-5} to 6.4×10^{-5}. Any effect of the low-loss sample on the cavity's stored energy, and thus on the Q, appears to be too small to affect the overall accuracy of the DRM technique.

Figure 5 shows the variation of negative frequency shift due to the PTFE shapes, plotted against their volume. For most of the objects, the shift was greater for the vertical mode (objects aligned with the z-axis) than for the horizontal (aligned with the x- or y-axis). For spheres the changes are similar for all modes, as expected. We can see that the average change in frequency follows a clear linear relationship, although the plots for the individual modes are much more variable. The corresponding results for the 3D-printed acrylic objects is shown in Figure 6. Again, the averaging removes the shape factor and linearises the plot.

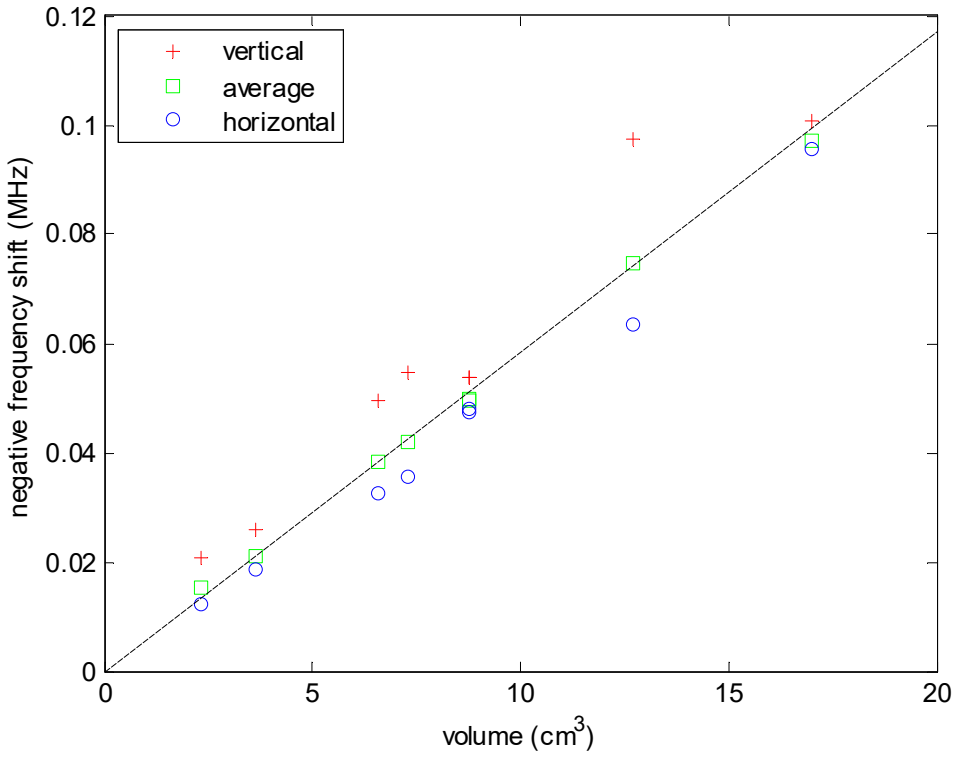

Figure 5. Variation of negative frequency shift with volume for PTFE shapes, showing individual modes and averaged data.

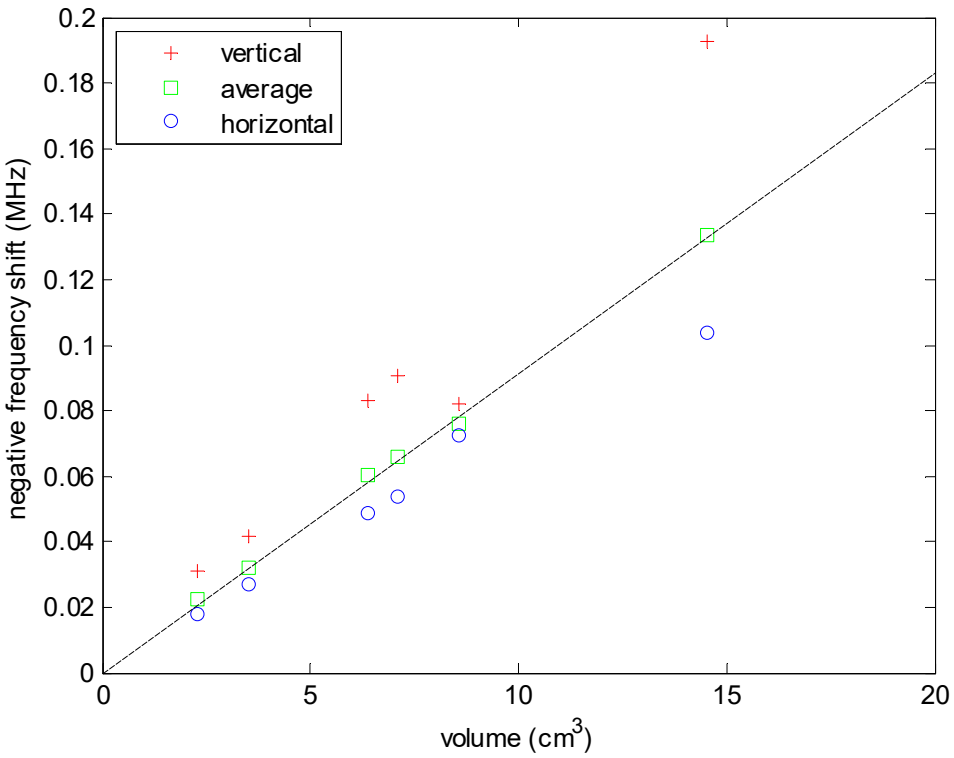

Figure 6. Variation of negative frequency shift with volume for 3D-printed acrylic shapes, showing individual modes and averaged data.

Figure 7 shows the complex permittivity of the acrylic material obtained from PTFE for the 5 solids, using the DRM procedure. It is evident that despite the differences in shape and size of the samples, the calculated dielectric constants and loss factors are close.

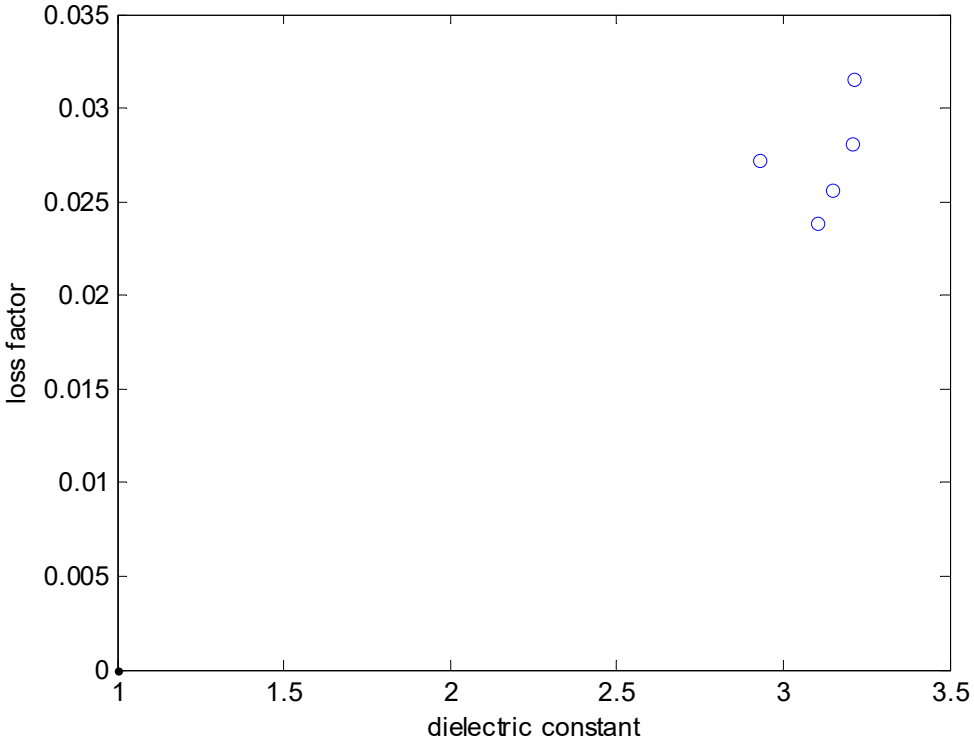

Figure 7. Complex permittivity of five acrylic objects obtained from PTFE replicas.

From these results, the mean values for the 3D printer material are $\varepsilon' = 3.12 \pm 0.12$ and $\varepsilon'' = 0.0272 \pm 0.0029$, the loss tangent $\varepsilon''/\varepsilon'$ being 0.00871 ± 0.00085 (Table 3). Data on the exact value of ε^* for this material was not found in the literature, but the value obtained by measurement is reasonable compared to acrylic polymers generally. From (6) the constant *C* is found to be 0.224 which is similar to values seen in other RCP measurements.

Now that we know the complex permittivity of the printer material, we can use this as the standard to calibrate other unknown materials. As a simple check, we can reverse the above procedure, and get ε^* of PTFE from ε^* of acrylic. Table 4 shows that this returns the original permittivity of 2.1 as expected.

Table 4. Permittivity of one material obtained from permittivity of another through DRM

Solid	Acrylic from PTFE, $\varepsilon^* = 2.1 - 0j$		PTFE from acrylic, $\varepsilon^* = 3.12 - 0.027j$	
	ε'	ε''	ε'	ε''
A, sphere	3.1483	0.0256	2.0890	-0.0009
B, short cylinder	3.1028	0.0238	2.1078	-0.0013
C, medium cylinder	3.2100	0.0280	2.0650	-0.0003
D, hollow cylinder	3.2155	0.0315	2.0629	0.0009
E, cone	2.9306	0.0272	2.1889	0.0017
Mean	3.12	0.027	2.10	4.6×10^{-5}
Standard deviation	0.12	0.0029	0.052	0.0013

The small negative values of ε'' for some of the PTFE shapes are worthy of comment as they imply a negative conductivity, which is physically impossible. However these deviations are less than the uncertainties in the measurement (see Section 7), and are clustered around zero with a very small mean. This suggests they are due to random experimental variation, rather than a systematic defect of the DRM technique.

6. Modification to model

Further tests on materials of known permittivity confirmed the linear variation of frequency shift with volume. However the variation of the α parameter with $\sum \Delta\Omega^{-1}$ in (7) was found to deviate slightly from linearity, leading to errors in the calculated permittivity.

To quantify this effect, further measurements were done on another set of objects that were chosen to be fairly close in shape and volume. Two spheres made of Perspex (methyl methacrylate), and PTFE sphere 'A' from Table 2 were included in the set. For higher values of dielectric constant, perfect spheres were not available, so instead specimens from one of the authors' mineral collections were included: two pieces of quartz (silica) and two of calcite (calcium carbonate).

Figure 8. Photograph showing (left to right): PTFE, Perspex, quartz and calcite. The sphere at the left is 25.6mm in diameter.

The materials are shown in Figure 8 and their properties listed in Table 5. We have now included the loss factor for PTFE although it is very small and makes little difference to the results. We have assumed quartz and calcite have sufficiently small loss factors that these can be taken as zero.

Table 5. Objects for testing linearity of DRM equation. Literature values from Kaye and Laby (1995) except Perspex from Bur (1985), as poly(methyl-methacrylate).

Solid	Volume (cm^3)	ε^* (literature)		ε^* (from modified model)	
		ε'	ε''	ε'	ε''
PTFE sphere A repeated 4 times	8.58	2.10	0.0004	2.087 2.083 2.077 2.099	-0.0004 0.0004 -0.0028 0.0020
Perspex sphere 1	8.18	2.65	0.0159	2.648	0.0171
Perspex sphere 2	8.18	2.65	0.0159	2.662	0.0177
Quartz crystal 1	11.78	3.90	0	4.17	0.0073
Quartz crystal 2	11.87	3.90	0	4.11	0.0047
Calcite crystal 1	7.70	8.25	0	7.81	-0.0119
Calcite crystal 2	8.61	8.25	0	7.65	-0.0118

From this data we derived a new prediction equation that includes a second-order term:

$$\alpha = \frac{\varepsilon^* - 1}{\varepsilon^* + 2} = p_0 + p_1 \frac{v_c}{v_s \sum \Delta\Omega^{-1}} + p_2 \left(\frac{v_c}{v_s \sum \Delta\Omega^{-1}} \right)^2 \qquad (11)$$

The value of p_0 must be zero so that the permittivity of air becomes exactly 1. The other coefficients of the polynomial were determined by the 'polyfit' function in Matlab to fit the experimental data. This gives p_1 = -0.4703 + 0.0004212j and p_2 = -0.05717 + 0.0002364j.

Figure 9 is a plot of the real part of α versus the real part of $\sum \Delta\Omega^{-1}$, showing the non-linear behaviour.

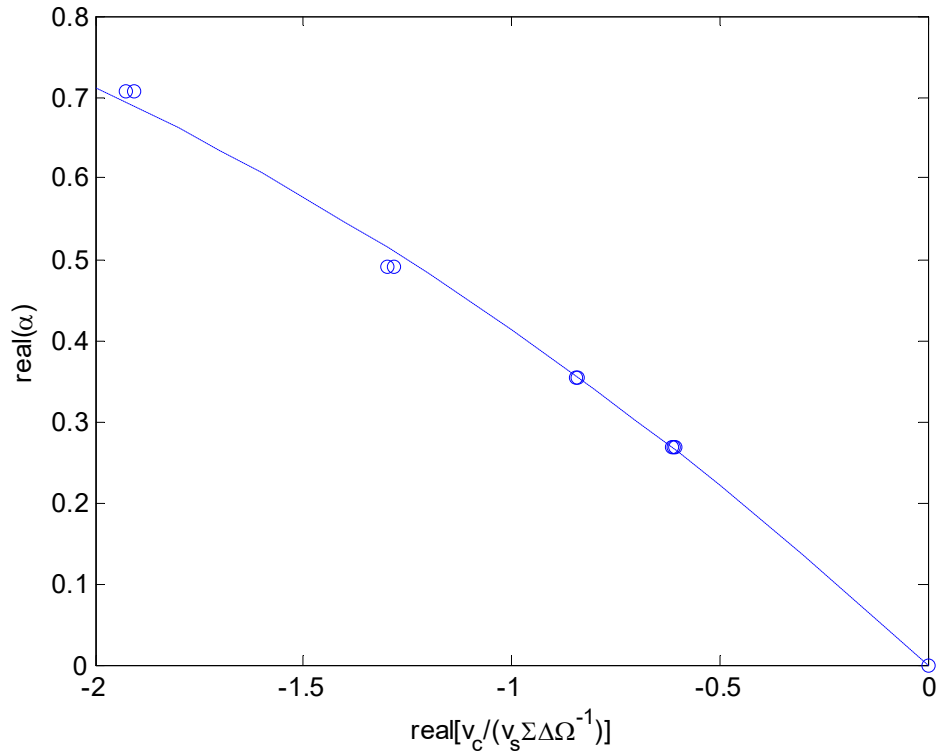

Figure 9. Variation of α with combined frequency shift, showing non-linearity

Applying (11) to the measured perturbations, and calculating complex permittivity from α, gives the values in the rightmost two columns of Table 4. The agreement with literature values is good for PTFE and Perspex and reasonable for quartz and calcite. The small deviations may be due to these crystals not being spherical, though we avoided shapes with large aspect ratios. Also note that no replicas were created here, and the permittivity was calculated just from the volume.

From (11) we get an improved value for the permittivity of the 3D printer material, which is now 2.94-0.0772j.

7. Application: archaeological objects

To demonstrate the feasibility of the proposed technique in a practical application, DRM was used to calculate the complex permittivity of two irregularly-shaped samples. For our initial study, we obtained samples of two materials that are commonly found on prehistoric and historic archaeological sites (rather than using actual archaeological artefacts). These were a sherd of

terracotta, from a broken ceramic vessel, and a piece of flint, similar to those made in ancient times for cutting and scoring: see Figure 10.

Figure 10. Photograph of pottery (left), flint and their 3D-printed replicas.

Table 6 lists the relevant details of the objects. Mass was obtained from an electronic balance with a precision of 0.01g. To estimate volume, we weighed the replicas of these objects, and assumed that the replicas had the same density as the 3D-printed acrylic sphere ('A' in Table 2), which we had previously calculated from mass/volume to be 1.179g/cm^3.

Table 6. Archaeological objects for testing repeatability of DRM technique

material	approximate shape	mass (g)	volume (cm^3)
terracotta pottery sherd	cuboid 30mm x 12mm x 6mm	3.78	2.02
flint chip	equilateral triangle side 20mm thickness 3mm	1.54	0.59

A 3D scan of each object was done to create a detailed representation of its surface, in .stl (stereolithography) and proprietary .wrp formats. Several replicas of each of these objects were created on the Stratasys Objet 24 printer. For each object, the complex permittivity was obtained by DRM three times, with a different replica being used in each measurement.

The baseline drift was found to be more of a problem than for the previous, larger test objects, owing to the smaller frequency shifts. The negative frequency changes for the pottery and its replicas were 0.016 to 0.040MHz, while for the flint and replicas the changes were only 0.0045 to 0.014MHz.

To reduce the errors due to drift even further, the 'loaded' measurements and the 'empty' measurements made either side of them were all time-stamped. It was assumed that any variation in the 'empty' parameters would be linear in time, and thus a weighted average of f_0, Q_0 at the time

of the loaded measurement was found by interpolating the 'before' and 'after' values accordingly. Table 7 shows an example calculation for one of the pottery replicas.

Table 7. example calculation of complex permittivity by DRM

parameter	replica pottery	original pottery
Δf_x (MHz)	-0.0162	-0.0190
Δf_y (MHz)	-0.0163	-0.0199
Δf_z (MHz)	-0.0280	-0.0402
ΔQ_x^{-1}	2.01×10^{-6}	3.56×10^{-6}
ΔQ_y^{-1}	1.75×10^{-6}	4.33×10^{-6}
ΔQ_z^{-1}	5.86×10^{-6}	1.52×10^{-5}
$\sum \Delta\Omega^{-1}$	-6.96×10^{4} - 2.08×10^{3}i	-5.57×10^{4} - 2.87×10^{3}i
v_s (cm^3)	2.03	2.03
α	0.393 - 0.00949i	0.473 - 0.0192i
ε*	2.94-0.0772i	**3.69 - 0.208i**

Figure 11 shows the results of the DRM measurements for the two 'archaeological' objects. It can be seen that there is some variation but also that the measurements cluster, and the two objects can be easily differentiated.

The measured dielectric constant of flint is close to, but slightly higher than, the value for quartz (3.9), which is not surprising as flint consists mostly of silica. The difference may be due to smaller amounts of other elements. Flint has a low loss factor, as expected. The dielectric constant of the pottery cannot be predicted without knowledge of the type of clay from which it was made, but the measured value is reasonable compared to typical values for ceramics. The pottery was unglazed, and therefore porous: it is likely that there was some ingress of water, which would explain the higher loss factor.

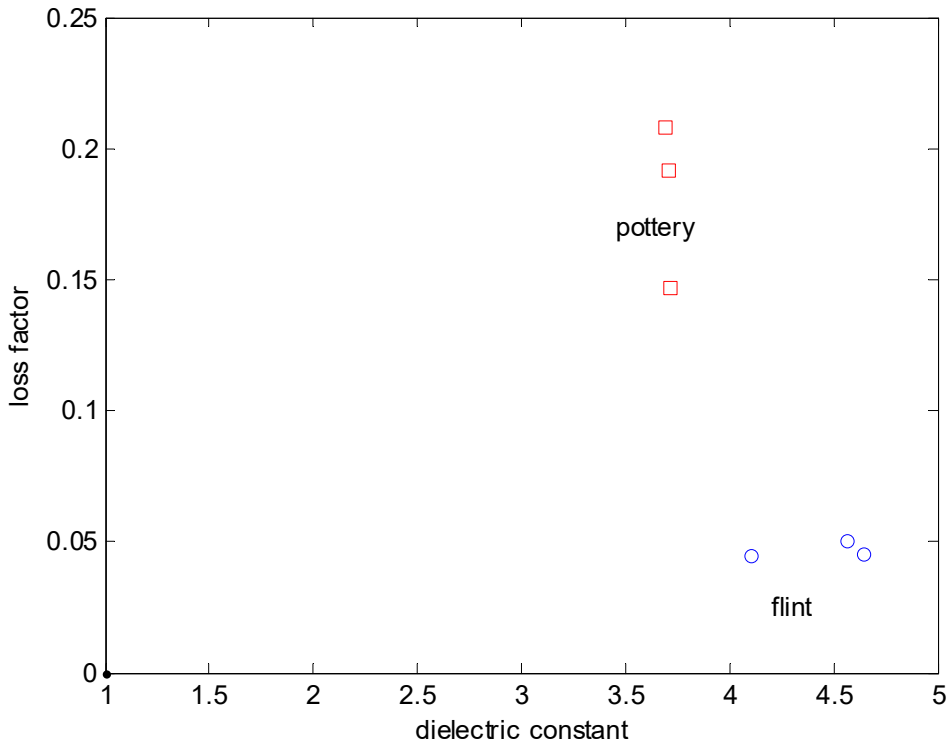

Figure 11. Calculated complex permittivity for two archaeological specimens, each obtained by DRM with three separate replicas.

To determine whether the uncertainties in the clustering were as expected, a Monte Carlo simulation was coded in Matlab. Values of the uncertainties in the input parameters, i.e. the frequency and Q-factor of the different modes with the cavity empty and loaded, were obtained by performing multiple measurements in quick succession. These were found to be 46Hz for the frequency of both modes, 6.6 for the Q of the horizontal (TE111) mode and 1.6 for the vertical (TM010) mode. The DRM calculations for one of the pottery replicas, and one of the flints, were then repeated 10^6 times, but with random changes in the input parameters corresponding to their measured uncertainties. The statistical variation in the population of ε^* was then examined.

The Monte Carlo simulation for pottery gave the uncertainty in ε' as 0.010 and in ε'' as 0.0065. For the smaller piece of flint the values were 0.052 and 0.031 respectively. The actual variation is somewhat larger than this, being 0.013 and 0.032 for pottery and 0.291 and 0.0032 for flint. There may be other sources of uncertainty that were not accounted for in the Monte Carlo model, and these will be investigated in ongoing research. The variation is still small compared to the differences between the two materials, particularly when real and imaginary parts are considered together on a 2D plot, enabling the materials to be easily distinguished.

8. Discussion

The above results show that DRM can give accurate, repeatable predictions of complex permittivity for low loss dielectrics. Although other researchers have investigated combining two or more perturbations, the exact formulation for completely removing the shape and volume factors has not, to our knowledge, been presented before, and thus represents a significant advance in the field of dielectric measurement. In principle it should also be applicable to materials with higher loss, but to demonstrate this will require further research.

So far we have only considered homogeneous materials, and for composites it would be harder to apply DRM (although still potentially useful) as the measured complex permittivity would be an effective value, intermediate between those of the constituents. Even if we are restricted to homogeneous materials, there are still many potential applications for this method of non-destructive testing. In archaeology, there are many examples of non-composite artefacts, particularly (but not exclusively) for prehistoric material, especially since organic components are rarely preserved. Stone tools, glass beads, jewellery and bone points are some examples.

The current equipment can deal with objects large enough to fit through the 46mm aperture in the cavity, while for smaller objects a limitation appears to be baseline drift. However the method could be extended to larger or smaller sizes by scaling the cavity: the ability to differentiate materials from their dielectric properties should exist over a broad range of frequencies.

A smaller chamber would be more sensitive because of the cavity volume term in (7). For example, increasing the frequency to 1GHz should improve the sensitivity by about 12 times, while allowing the cavity size to be 43% of the current chamber in all dimensions. It need not be a cylinder, and a cuboidal cavity with all sides close in length, but not identical (to separate the modes) might be easier to build.

The thermal drift in the 'empty' measurements could be reduced further by (a) operating in a temperature controlled room or (b) placing insulation, such as expanded polystyrene sheets, on the cavity walls.

A third pair of switchable antennas can be added, to get all the x, y and z perturbations without rotating the sample holder. Alternatively, with a more complicated mechanical device to rotate the sample about two perpendicular axes, we could have a DRM system with just a single resonant mode.

Currently we are comparing the replicas made on different models of 3D printer, to determine which shows the best repeatability. We are also extending our research to a wider variety of artefact materials.

DRM is a non-destructive, non-invasive method using low power microwaves. The only physical effect on the sample is heating from the absorption of electromagnetic energy. However with the sub-milliwatt power levels from the VNA, the temperature rise within a typical measurement time will be insignificant.

9. Conclusion

The DRM technique will be a useful non-destructive method of obtaining the dielectric properties of precious or fragile materials. It provides two separate parameters, the dielectric constant and loss factor, to characterise non-metallic materials, and thus aid in their identification.

DRM relies on the microwave fields fully penetrating the sample, and so provides a bulk measurement that depends on the whole volume. In this way it would complement other techniques such as LA-ICP-MS and micro X-ray fluorescence (micro-XRF) that rely on probing the object's surface.

Applications of the technique include object identification of recently excavated artefacts, as well as the analysis and characterisation of objects in existing museum collections. Examples of materials that might be tested, in addition to pieces of ceramic or flint, are gemstones and glasses, which can be hard to distinguish, and similarly elephant ivory from bone, or teeth of other animal species.

Thus, this application is likely to have use for other sectors, such as customs, and animal protection and environmental agencies.

A final advantage of DRM is that it leaves a physical 3D replica of the measured object as a bonus: this feature could be attractive for museums and other educational institutes where artefact replicas are now frequently used. Museums now run schemes by which members of the public can have their archaeological finds measured and recorded (Portable Antiquities Scheme 2018), and the opportunity to have a DRM measurement and replica object would encourage participation. DRM thus has a role in teaching and outreach as well as scientific investigation.

Acknowledgement

We thank Mr George Wooley for making the PTFE and acrylic shapes listed in Table 2.

References

Bur, A.J., 1985. Dielectric properties of polymers at microwave frequencies: a review. *Polymer*, **26**(7), pp.963-977

Chen, L., Ong, C.K. and Tan, B.T.G., 1999. Amendment of cavity perturbation method for permittivity measurement of extremely low-loss dielectrics. *IEEE Transactions on Instrumentation and Measurement*, *48*(6), pp.1031-1037.

Evans, S., Rachman, M.J. and Pegg, D.E., 1992. Design of a UHF applicator for rewarming of cryopreserved biomaterials. *IEEE Transactions on Biomedical Engineering*, *39*(3), pp.217-225.

Evans, A.A., J.L. Langer., R.E. Donahue., Y.B. Wolframm. & W.A. Lovis. 2010. Lithic raw material sourcing and the assessment of Mesolithic landscape organization and mobility strategies in northern England *Holocene* **20**. SAGE Publications Ltd: 1157–63.

Fitzpatrick, S.M., W.R. Dickinson. & G. Clark. 2003. Ceramic petrography and cultural interaction in Palau, Micronesia *Journal of archaeological science* **30**: 1175–84.

Freestone, I.C. 2006. Glass production in Late Antiquity and the Early Islamic period: a geochemical perspective *Geological Society, London, Special Publications* **257**. Geological Society of London: 201–16.

Gregory, AP and Clarke, RN 2006 'A review of RF and microwave techniques for dielectric measurements on polar liquids,' *IEEE Transactions on Dielectrics and Electrical Insulation*, vol. **13**, pp.727-743

Harrington R F 1961, *Time Harmonic Electromagnetic Fields,* Wiley, New York, Ch. 7.

Horner F, Taylor T A, Dunsmuir R, Lamb J and Jackson W 1946. 'Resonance methods of dielectric measurement at centimetre wavelengths.' *J. IEE* **93 III** pp53-68

Kaatze, U, 2012. Measuring the dielectric properties of materials. Ninety-year development from low-frequency techniques to broadband spectroscopy and high-frequency imaging. Measurement Science and Technology, **24**(1), p.012005.

Kaye G W C and Laby T H 1995 *Tables of Physical and Chemical Constants and Some Mathematical Functions* 16th Edition, Longman, available online at www.kayelaby.npl.co.uk/ (accessed 30th August 2018)

Kraszewski, A.W., Nelson, S.O. and You, T.S., 1990. Use of a microwave cavity for sensing dielectric properties of arbitrarily shaped biological objects. *IEEE Transactions on Microwave Theory and Techniques*, **38**(7), pp.858-863.

Kraszewski A W and Nelson S O 1996. 'Resonant cavity perturbation: some new applications of an old measuring technique' *J. Microwave Power* vol. **31**, pp 178-187.

Müller, K. & I. Reiche. 2011. Differentiation of archaeological ivory and bone materials by micro-PIXE/PIGE with emphasis on two Upper Palaeolithic key sites: Abri Pataud and Isturitz, France *Journal of archaeological science* **38**: 3234–43.

Nuutinen J, Ikäheimo R and Lahtinen T 2004, 'Validation of a new dielectric device to assess changes of tissue water in skin and subcutaneous fat' Physiol. Meas. 25 pp 447-454.

B. Oldroyd, M. P. Robinson, E. Lindley, L. Rhodes, K Hind 2015. 'Resonant cavity perturbation: a promising new method for the assessment of total body water in children' *Physiol. Meas.* **36** pp 2503-2517

Portable Antiquities Scheme 2018, Portable Antiquities Scheme Website, https://finds.org.uk/, accessed 31st August 2018.

Rachman, M.J., Evans, S. and Pegg, D.E., 1992. Experimental results on the rewarming of a cryopreserved organ phantom in a UHF field. *Journal of Biomedical Engineering*, *14*(5), pp.397-403.

M P Robinson, I D Flintoft, L Dawson, J Clegg, J G Truscott and X Zhu 2010, 'Application of Resonant Cavity Perturbation to in-vivo Segmental Hydration Analysis' *Meas. Sci. Technol.* **21** pp 015804.1-015804.10

M P Robinson and J Clegg 2008, 'Calibration of Biomedical Dielectric Sensors Optimised using Genetic Algorithm', Proceedings of the XXIX General Assembly of the International Union of Radio Science (URSI), Chicago, Illinois, USA, August 7-16, Paper No. K01.1

M P Robinson and D E Pegg 1999. 'Rapid electromagnetic warming of cells and tissues' *IEEE Trans Bio-Med. Eng.* **46** pp 1413-1425.

Sheen, J., 2007. Amendment of cavity perturbation technique for loss tangent measurement at microwave frequencies. *Journal of Applied Physics*, *102*(1), p.014102.

Truncher, J., M.D. Glascock. & M. Neff. 1998. Steatite source characterization in eastern North America: new results using instrumental neutron activation analysis *Archaeometry* **40**: 23–44.

von Holstein, I.C., S.P. Ashby., N.L. van Doorn., S.M. Sachs., M. Buckley., M. Meirai., I. Barnes., A. Brundle. & M.J. Collins. 2014. Searching for Scandinavians in pre-Viking Scotland: molecular fingerprinting of Early Medieval combs *Journal of archaeological science* **41**: 1–6.